Physica A 465 (2017) 742–753

Contents lists available at ScienceDirect

Physica A

journal homepage: www.elsevier.com/locate/physa

Lattice Boltzmann simulations of convection heat transfer in porous media

Qing Liu, Ya-Ling He *

Key Laboratory of Thermo-Fluid Science and Engineering of Ministry of Education, School of Energy and Power Engineering, Xi'an Jiaotong University, Xi'an, Shaanxi, 710049, China

HIGHLIGHTS

- A non-orthogonal MRT-LB method is developed for convection heat transfer in porous media.
- The proposed method is based on the generalized non-Darcy model.
- Two LB models are constructed: one is the DDF-MRT model, and the other is the hybrid MRT-FDM model.
- The proposed method can be served as an accurate and efficient method for convection heat transfer in porous media.

ARTICLE INFO

Article history:
Received 25 February 2016
Received in revised form 22 June 2016
Available online 24 August 2016

Keywords:
Lattice Boltzmann method
Non-orthogonal MRT model
Convection heat transfer
Porous media
Generalized non-Darcy model
Hybrid approach

ABSTRACT

A non-orthogonal multiple-relaxation-time (MRT) lattice Boltzmann (LB) method is developed to study convection heat transfer in porous media at the representative elementary volume scale based on the generalized non-Darcy model. In the method, two different LB models are constructed: one is constructed in the framework of the double-distribution-function approach, and the other is constructed in the framework of the hybrid approach. In particular, the transformation matrices used in the MRT-LB models are non-orthogonal matrices. The present method is applied to study mixed convection flow in a porous channel and natural convection flow in a porous cavity. It is found that the numerical results are in good agreement with the analytical solutions and/or other results reported in previous studies. Furthermore, the non-orthogonal MRT-LB method shows better numerical stability in comparison with the BGK-LB method.

1. Introduction

Fluid flow and convection heat transfer in porous media have attracted considerable attention due to their fundamental nature and broad range of applications in many fields of science and engineering. Consequently, fluid flow and convection heat transfer in porous media have been studied extensively by using theoretical, experimental, and numerical methods [1,2]. Fluid flow and convection heat transfer in porous media usually involve three scales, i.e., the domain scale, the representative elementary volume (REV) scale, and the pore scale. In the last several decades, various traditional numerical methods have been developed to study convection heat transfer processes in porous media at the REV scale based on some semi-empirical models, such as the Darcy model, the Brinkman-extended Darcy model, the Forchheimer-extended Darcy model, and the generalized non-Darcy model (also called the Brinkman–Forchheimer-extended Darcy model) [2–6].

* Corresponding author.
E-mail address: yalinghe@mail.xjtu.edu.cn (Y.-L. He).

http://dx.doi.org/10.1016/j.physa.2016.08.010
0378-4371/

The lattice Boltzmann (LB) method [7–11], as a mesoscopic numerical approach originated from the lattice-gas automata (LGA) method [12], has achieved great success in simulating fluid flows and modeling physics in fluids [13–22]. Unlike traditional numerical methods based on a direct discretization of macroscopic continuum equations, the LB method is based on mesoscopic kinetic equation for single-particle distribution function. As reported by Succi [23,24], the LB method has some attractive advantages over traditional numerical methods due to its kinetic background: (i) non-linearity (collision process) is local and non-locality (streaming process) is linear, whereas the transport term $\mathbf{u}\cdot\nabla\mathbf{u}$ in the Navier–Stokes equations is non-linear and non-local at a time; (ii) streaming is exact; (iii) the strain tensor and the fluid pressure can be calculated locally; (iv) complex boundary conditions can be easily formulated in terms of the elementary mechanical rules; (v) nearly ideal for parallel computing with very low communication/computation ratio.

The LB method has also been successfully applied to study fluid flow and heat transfer in porous media. The LB models for fluid flow and heat transfer in porous media can be generally classified into two categories, i.e., the pore scale method [25–29] and the REV scale method [30–39]. In fact, the LB method was already applied to study three-dimensional porous flows at the pore scale by Succi et al. in 1989 [25]. Later studies [26–28] demonstrated the reliability of the LB method in modeling fluid flows in porous media. Very recently, Prestininzi et al. [29] have brought factual evidence that the Bhatnagar–Gross–Krook (BGK) LB model is capable of modeling Darcy flow through arrays of equal spheres within a few percent accuracy. In the pore scale method, fluid flow and heat transfer in the pores of the medium is directly modeled by the standard LB method, and the interaction between solid and fluid phases is realized by using the no-slip bounce-back rule. The detailed flow information of the pores can be obtained, which can be utilized to investigate macroscopic relations.

In the REV scale method, an additional term accounting for the presence of a porous medium is incorporated into the LB equation by using some appropriate forcing schemes based on some semi-empirical models (e.g., Darcy model [33], Brinkman-extended Darcy model [30–32], and generalized non-Darcy model [34–39]). Based on the generalized non-Darcy model [6], Guo and Zhao [34] developed a generalized LB model for studying incompressible porous flows. In the generalized LB model, the porosity is incorporated into the equilibrium distribution function, and a forcing term is added into the LB equation to account for the linear and nonlinear matrix drag forces. Subsequently, the generalized LB model was extended to study convection heat transfer in porous media [36,37]. After nearly two decades of development, the REV scale method has been developed into a numerically accurate and computationally efficient numerical method for studying fluid flow and convection heat transfer in porous media on large scales.

In the LB community, the BGK model [10,11] is still the most popular one owning to its simplicity. However, the single-relaxation-time assumption of the BGK model obviously comes with several limitations, e.g., it usually suffers from numerical instability at low viscosity (the relaxation time is close to 0.5), and it is restricted to fluids with isotropic diffusion coefficient. One way to overcome the defects of the BGK model is to use the multiple-relaxation-time (MRT) model proposed by d'Humières in 1992 [40], which is an important extension of the matrix LB method developed by Higuera et al. [9]. Actually the basic idea of any MRT scheme is originated from the work of Higuera et al. [9]. It has been widely accepted that the MRT model can significantly improve the numerical stability of the LB schemes by carefully separating the relaxation rates of the hydrodynamic (conserved) and kinetic (non-conserved) moments [41–44]. In addition, the number of tunable parameters in the MRT model is sufficient to handle problems with anisotropic diffusion coefficient [45,46]. In our previous study [39], a thermal MRT-LB model was developed for simulating convection heat transfer in porous media at the REV scale in the framework of the double-distribution-function (DDF) approach. In the model, the MRT-LB equations are proposed based on orthogonal transformation matrices. However, as reported in Refs. [47,48], the transformation matrix of the MRT-LB model is not necessary to be an orthogonal one, i.e., the MRT-LB model can be developed based on non-orthogonal transformation matrix, which results in the so-called non-orthogonal MRT-LB model. In the non-orthogonal MRT-LB model, the Gram–Schmidt orthogonalization process is not needed. Compared with the orthogonal transformation matrix, the non-orthogonal transformation matrix contains more zero elements, which makes the non-orthogonal MRT-LB model simpler and more efficient than the classical orthogonal MRT-LB model [41].

In this paper, we aim to present a non-orthogonal MRT-LB method for convection heat transfer in porous media at the REV scale. In the method, two different LB models are constructed: one is constructed in the framework of the DDF approach [48–51], and the other is constructed in the framework of the hybrid approach [42]. The rest of this paper is organized as follows. The macroscopic governing equations are briefly described in Section 2. The non-orthogonal MRT-LB method is presented in Section 3. The numerical results and some discussions are given in Section 4. Finally, a brief conclusion is made in Section 5.

2. Macroscopic governing equations

For fluid flow and convection heat transfer in a homogeneous, isotropic and fluid-saturated porous medium at the REV scale, based on the generalized non-Darcy model, the macroscopic governing equations under local thermal equilibrium condition can be written as follows [2,6]:

$$\nabla\cdot\mathbf{u}=0, \tag{1}$$

$$\frac{\partial\mathbf{u}}{\partial t}+(\mathbf{u}\cdot\nabla)\left(\frac{\mathbf{u}}{\phi}\right)=-\frac{1}{\rho_0}\nabla(\phi p)+\upsilon_e\nabla^2\mathbf{u}+\mathbf{F}, \tag{2}$$

$$\sigma \frac{\partial T}{\partial t} + \mathbf{u} \cdot \nabla T = \nabla \cdot (\alpha_e \nabla T), \tag{3}$$

where ρ_0 is the mean fluid density, $\mathbf{u}$, T, and p are the volume-averaged fluid velocity, temperature, and pressure, respectively, ϕ is the porosity of the porous medium, υ_e is the effective kinematic viscosity, σ is the thermal capacity ratio between solid and fluid phases, and α_e is the effective thermal diffusivity. $\mathbf{F} = (F_x,\ F_y)$ denotes the total body force induced by the porous media and other external forces, which can be expressed as [5]

$$\mathbf{F} = -\frac{\phi \upsilon}{K}\mathbf{u} - \frac{\phi F_\phi}{\sqrt{K}} |\mathbf{u}| \mathbf{u} + \phi \mathbf{G}, \tag{4}$$

where K is the permeability of the porous medium, υ is the kinematic viscosity of the fluid (υ is not necessarily the same as υ_e), and $|\mathbf{u}| = \sqrt{u_x^2 + u_y^2}$, in which u_x and u_y are the x- and y-components of the fluid velocity $\mathbf{u}$, respectively. Based on Boussinesq approximation, the body force $\mathbf{G}$ is given by $\mathbf{G} = g\beta (T - T_0)\mathbf{j}$, where g is the gravitational acceleration, β is the thermal expansion coefficient, T_0 is the reference temperature, and $\mathbf{j}$ is the unit vector in the vertical direction.

For flow over spherical particles, according to Ergun's experimental investigations [52], the geometric function F_ϕ and the permeability K can be expressed as [4]

$$F_\phi = \frac{1.75}{\sqrt{150\phi^3}}, \qquad K = \frac{\phi^3 d_p^2}{150 (1-\phi)^2}, \tag{5}$$

where d_p is the diameter of the spherical particle.

In addition to the porosity ϕ and the thermal capacity ratio σ, convection heat transfer in porous media governed by Eqs. (1)–(3) is characterized by several dimensionless parameters: the Darcy number $Da = K/L^2$, the Rayleigh number $Ra = g\beta\Delta T L^3/(\upsilon\alpha)$, the Reynolds number $Re = LU/\upsilon$ (for mixed convection flow), the Prandtl number $Pr = \upsilon/\alpha$, the viscosity ratio $J = \upsilon_e/\upsilon$, and the thermal diffusivity ratio $\gamma = \alpha_e/\alpha$, where L is the characteristic length, U is the characteristic velocity, and α is the thermal diffusivity of the fluid.

3. Non-orthogonal MRT-LB method for convection heat transfer in porous media

3.1. Flow field

For two-dimensional (2D) porous flows considered in this work, the two-dimensional nine-velocity (D2Q9) lattice is employed. The nine discrete velocities $\{\mathbf{e}_i | i = 0, 1, \ldots, 8\}$ of the D2Q9 lattice are given by [11]

$$\mathbf{e}_i = \begin{cases} (0, 0), & i = 0, \\ (\cos[(i-1)\pi/2], \sin[(i-1)\pi/2])\, c, & i = 1\text{–}4, \\ (\cos[(2i-9)\pi/4], \sin[(2i-9)\pi/4])\, \sqrt{2}c, & i = 5\text{–}8, \end{cases} \tag{6}$$

where $c = \delta_x/\delta_t$ is the lattice speed with δ_t and δ_x being the discrete time step and lattice spacing, respectively. The lattice speed c is set to be 1 ($\delta_x = \delta_t$) in this work.

The MRT-LB equation with a semi-implicit treatment of the forcing term can be written as [43,48]

$$f_i(\mathbf{x} + \mathbf{e}_i\delta_t, t + \delta_t) - f_i(\mathbf{x}, t) = -\tilde{\Lambda}_{ij}\left(f_j - f_j^{eq}\right)\big|_{(\mathbf{x},t)} + \frac{\delta_t}{2}\left[S_i|_{(\mathbf{x},t)} + S_i|_{(\mathbf{x}+\mathbf{e}_i\delta_t, t+\delta_t)}\right], \tag{7}$$

where $f_i(\mathbf{x}, t)$ is the density distribution function, $f_i^{eq}(\mathbf{x}, t)$ is the equilibrium density distribution function, S_i is the forcing term, and $\tilde{\mathbf{\Lambda}}$ is the collision matrix. Eq. (7) is implicit and cannot be directly implemented in computations. By using a transformed distribution function $\bar{f}_i = f_i - 0.5\delta_t S_i$, the following explicit MRT-LB equation can be obtained:

$$\bar{f}_i(\mathbf{x} + \mathbf{e}_i\delta_t, t + \delta_t) = \bar{f}_i(\mathbf{x}, t) - \tilde{\Lambda}_{ij}\left(\bar{f}_j - f_j^{eq}\right)\big|_{(\mathbf{x},t)} + \delta_t\left(S_i - 0.5\tilde{\Lambda}_{ij}S_j\right)\big|_{(\mathbf{x},t)}. \tag{8}$$

MRT-LB equation (8) consists of two steps: the collision process and streaming process. Through a transformation matrix $\mathbf{M}$, the collision process can be executed in the moment space:

$$\bar{\mathbf{m}}^*(\mathbf{x}, t) = \bar{\mathbf{m}}(\mathbf{x}, t) - \mathbf{\Lambda}\left(\bar{\mathbf{m}} - \mathbf{m}^{eq}\right)\big|_{(\mathbf{x},t)} + \delta_t\left(\mathbf{I} - \frac{\mathbf{\Lambda}}{2}\right)\tilde{\mathbf{S}}, \tag{9}$$

while the streaming process is still carried out in the velocity space:

$$\bar{f}_i(\mathbf{x} + \mathbf{e}_i\delta_t, t + \delta_t) = \bar{f}_i^*(\mathbf{x}, t), \tag{10}$$

where $\mathbf{\Lambda} = \mathbf{M}\tilde{\mathbf{\Lambda}}\mathbf{M}^{-1} = \mathrm{diag}\,(s_0, s_1, \ldots, s_8)$ is a diagonal relaxation matrix ($\mathbf{M}$ is a non-orthogonal transformation matrix, and $\{s_i\}$ are relaxation rates), and $\mathbf{I}$ is the identity matrix. The bold-face symbols $\mathbf{m}$, $\bar{\mathbf{m}}$, $\mathbf{m}^{eq}$ and $\tilde{\mathbf{S}}$ denote 9-dimensional column vectors of moments as follows:

$$\mathbf{m} = |m\rangle = \mathbf{M}\mathbf{f}, \qquad \bar{\mathbf{m}} = |\bar{m}\rangle = \mathbf{M}\bar{\mathbf{f}}, \qquad \mathbf{m}^{eq} = \left|m^{eq}\right\rangle = \mathbf{M}\mathbf{f}^{eq}, \qquad \tilde{\mathbf{S}} = \left|\tilde{S}\right\rangle = \mathbf{M}\mathbf{S}, \tag{11}$$

where $\mathbf{f} = |f\rangle$, $\bar{\mathbf{f}} = \left|\bar{f}\right\rangle$, $\mathbf{f}^{eq} = |f^{eq}\rangle$, and $\mathbf{S} = |S\rangle$. For brevity, the notation $|\cdot\rangle$ is employed to denote a 9-dimensional column vector, e.g., $|m\rangle = (m_0, m_1, \ldots, m_8)^T$. The post-collision distribution functions $\left\{\bar{f}_i^*\right\}$ can be determined by $\bar{\mathbf{f}}^* = \left|\bar{f}^*\right\rangle = \mathbf{M}^{-1}\bar{\mathbf{m}}^*$. The non-orthogonal transformation matrix $\mathbf{M}$ is defined by ($c = 1$) [47,48]

$$\begin{aligned}\mathbf{M} &= \left[|1\rangle, |e_x\rangle, \left|e_y\right\rangle, \left|e_x^2 + e_y^2\right\rangle, \left|e_x^2 - e_y^2\right\rangle, \left|e_x e_y\right\rangle, \left|e_x^2 e_y\right\rangle, \left|e_x e_y^2\right\rangle, \left|e_x^2 e_y^2\right\rangle\right]^T \\ &= \begin{bmatrix} 1 & 1 & 1 & 1 & 1 & 1 & 1 & 1 & 1 \\ 0 & 1 & 0 & -1 & 0 & 1 & -1 & -1 & 1 \\ 0 & 0 & 1 & 0 & -1 & 1 & 1 & -1 & -1 \\ 0 & 1 & 1 & 1 & 1 & 2 & 2 & 2 & 2 \\ 0 & 1 & -1 & 1 & -1 & 0 & 0 & 0 & 0 \\ 0 & 0 & 0 & 0 & 0 & 1 & -1 & 1 & -1 \\ 0 & 0 & 0 & 0 & 0 & 1 & 1 & -1 & -1 \\ 0 & 0 & 0 & 0 & 0 & 1 & -1 & -1 & 1 \\ 0 & 0 & 0 & 0 & 0 & 1 & 1 & 1 & 1 \end{bmatrix}. \end{aligned} \tag{12}$$

With the transformation matrix $\mathbf{M}$ given above, the moments $\mathbf{m}$ and $\bar{\mathbf{m}}$ are defined as follows:

$$\mathbf{m} = |m\rangle = \left(\rho, j_x, j_y, e, p_{xx}, p_{xy}, q_{xxy}, q_{xyy}, \varepsilon\right)^T, \tag{13}$$

$$\bar{\mathbf{m}} = |\bar{m}\rangle = \left(\rho, j_x - \frac{\delta_t}{2}\rho F_x, j_y - \frac{\delta_t}{2}\rho F_y, \bar{e}, \bar{p}_{xx}, \bar{p}_{xy}, \bar{q}_{xxy}, \bar{q}_{xyy}, \bar{\varepsilon}\right)^T, \tag{14}$$

where $j_x = \rho u_x$ and $j_y = \rho u_y$ are x- and y-components of the momentum $\mathbf{j} = \rho\mathbf{u} = \left(j_x, j_y\right)$, and $\mathbf{m} = \bar{\mathbf{m}} + 0.5\delta_t\tilde{\mathbf{S}}$ ($\bar{f}_i = f_i - 0.5\delta_t S_i$). The equilibrium moments $\left\{m_i^{eq} \middle| i = 0, 1, \ldots, 8\right\}$ are given by

$$\begin{aligned} &m_0^{eq} = \rho, \qquad m_1^{eq} = \rho u_x, \qquad m_2^{eq} = \rho u_y, \qquad m_3^{eq} = \frac{2}{3}\rho + \frac{\rho\left(u_x^2 + u_y^2\right)}{\phi}, \qquad m_4^{eq} = \frac{\rho\left(u_x^2 - u_y^2\right)}{\phi}, \\ &m_5^{eq} = \frac{\rho u_x u_y}{\phi}, \qquad m_6^{eq} = \frac{1}{3}\rho u_y, \qquad m_7^{eq} = \frac{1}{3}\rho u_x, \qquad m_8^{eq} = \frac{1}{9}\rho + \frac{1}{3}\frac{\rho\left(u_x^2 + u_y^2\right)}{\phi}. \end{aligned} \tag{15}$$

The equilibrium distribution function f_i^{eq} in the velocity space is given by [34]

$$f_i^{eq} = \omega_i\rho\left[1 + \frac{\mathbf{e}_i\cdot\mathbf{u}}{c_s^2} + \frac{\mathbf{u}\mathbf{u} : \left(\mathbf{e}_i\mathbf{e}_i - c_s^2\mathbf{I}\right)}{2\phi c_s^4}\right], \tag{16}$$

where $\omega_0 = 4/9$, $\omega_i = 1/9$ for $i = 1 - 4$, $\omega_i = 1/36$ for $i = 5 - 8$, and $c_s = c/\sqrt{3}$ is the lattice sound speed of the D2Q9 model. The components of the forcing term $\tilde{\mathbf{S}}$ are given as follows:

$$\begin{aligned} &\tilde{S}_0 = 0, \qquad \tilde{S}_1 = \rho F_x, \qquad \tilde{S}_2 = \rho F_y, \qquad \tilde{S}_3 = \frac{2\rho\left(u_x F_x + u_y F_y\right)}{\phi}, \qquad \tilde{S}_4 = \frac{2\rho\left(u_x F_x - u_y F_y\right)}{\phi}, \\ &\tilde{S}_5 = \frac{\rho\left(u_x F_y + u_y F_x\right)}{\phi}, \qquad \tilde{S}_6 = \frac{1}{3}\rho F_y, \qquad \tilde{S}_7 = \frac{1}{3}\rho F_x, \qquad \tilde{S}_8 = \frac{2}{3}\frac{\rho\left(u_x F_y + u_y F_x\right)}{\phi}. \end{aligned} \tag{17}$$

The diagonal relaxation matrix $\mathbf{\Lambda}$ is given by

$$\begin{aligned}\mathbf{\Lambda} &= \mathrm{diag}\,(s_0, s_1, s_2, s_3, s_4, s_5, s_6, s_7, s_8) \\ &= \mathrm{diag}\left(1, 1, 1, s_e, s_\upsilon, s_\upsilon, s_q, s_q, s_\varepsilon\right). \end{aligned} \tag{18}$$

The macroscopic fluid density ρ and velocity $\mathbf{u}$ are given by

$$\rho = \sum_{i=0}^{8} f_i = \sum_{i=0}^{8}\bar{f}_i, \tag{19}$$

$$\rho\mathbf{u} = \sum_{i=0}^{8}\mathbf{e}_i f_i = \sum_{i=0}^{8}\mathbf{e}_i\bar{f}_i + \frac{\delta_t}{2}\rho\mathbf{F}. \tag{20}$$

The macroscopic fluid pressure p is defined as $p = \rho c_s^2/\phi$. Note that Eq. (20) is a nonlinear equation for the velocity $\mathbf{u}$. By introducing a temporal velocity $\mathbf{v}$, the macroscopic fluid velocity $\mathbf{u}$ can be calculated by

$$\mathbf{u} = \frac{\mathbf{v}}{l_0 + \sqrt{l_0^2 + l_1 |\mathbf{v}|}}, \tag{21}$$

where

$$\mathbf{v} = \sum_{i=0}^{8} \mathbf{e}_i f_i/\rho_0 + \frac{\delta_t}{2}\phi\mathbf{G}, \qquad l_0 = \frac{1}{2}\left(1 + \phi\frac{\delta_t}{2}\frac{\upsilon}{K}\right), \qquad l_1 = \phi\frac{\delta_t}{2}\frac{F_\phi}{\sqrt{K}}. \tag{22}$$

The macroscopic fluid pressure p is defined as $p = \rho c_s^2/\phi$. Through the Chapman–Enskog analysis, the generalized Navier–Stokes equations (1) and (2) can be recovered from the MRT-LB equation (8) in the incompressible limit. The effective kinetic viscosity υ_e is defined as $\upsilon_e = c_s^2\,(\tau_\upsilon - 0.5)\,\delta_t$ with $s_{4,5} = s_\upsilon = 1/\tau_\upsilon$.

3.2. Temperature field

In the past two decades, many attempts have been made to develop LB models for solving the convection–diffusion equation (or internal-energy equation) [45,46,48–51]. In this work, the two-dimensional five-velocity (D2Q5) non-orthogonal MRT-LB model [48] and the finite difference scheme [42] are employed to solve the temperature field governed by Eq. (3).

3.2.1. D2Q5 non-orthogonal MRT-LB equation

For the temperature field, the D2Q5 non-orthogonal MRT-LB equation is given by [48]

$$g_i\left(\mathbf{x} + \mathbf{e}_i\delta_t, t + \delta_t\right) - g_i\left(\mathbf{x}, t\right) = -\left(\mathbf{N}^{-1}\mathbf{Q}\mathbf{N}\right)_{ij}\left(g_j - g_j^{eq}\right)\Big|_{(\mathbf{x},t)}, \tag{23}$$

where $g_i\left(\mathbf{x}, t\right)$ is the temperature distribution function, $g_i^{eq}\left(\mathbf{x}, t\right)$ is the equilibrium distribution function, $\mathbf{Q}$ is the relaxation matrix, and $\mathbf{N}$ is the non-orthogonal transformation matrix. Through the transformation matrix $\mathbf{N}$, the collision process of MRT-LB equation (23) can be executed in the moment space:

$$\mathbf{n}^*\left(\mathbf{x}, t\right) = \mathbf{n}\left(\mathbf{x}, t\right) - \mathbf{Q}\left(\mathbf{n} - \mathbf{n}^{eq}\right)\Big|_{(\mathbf{x},t)}, \tag{24}$$

while the streaming process is carried out in the velocity space:

$$g_i\left(\mathbf{x} + \mathbf{e}_i\delta_t, t + \delta_t\right) = g_i^*\left(\mathbf{x}, t\right), \tag{25}$$

where $\mathbf{n}$ and $\mathbf{n}^{eq}$ are vectors defined by $\mathbf{n} = |n\rangle = \mathbf{N}\mathbf{g}$ and $\mathbf{n}^{eq} = |n^{eq}\rangle = \mathbf{N}\mathbf{g}^{eq}$, respectively. The post-collision distribution functions $\left\{g_i^*\right\}$ are determined by $\mathbf{g}^* = |g^*\rangle = \mathbf{N}^{-1}\mathbf{n}^*$. The five discrete velocities $\{\mathbf{e}_i|\, i = 0, 1, \ldots, 4\}$ of the D2Q5 lattice are given in Eq. (6). For D2Q5 model, the non-orthogonal transformation matrix $\mathbf{N}$ can be defined as [48]

$$\begin{aligned}\mathbf{N} &= \left[|1\rangle, |e_x\rangle, \left|e_y\right\rangle, \left|e_x^2 + e_y^2\right\rangle, \left|e_x^2 - e_y^2\right\rangle\right]^T \\ &= \begin{bmatrix} 1 & 1 & 1 & 1 & 1 \\ 0 & 1 & 0 & -1 & 0 \\ 0 & 0 & 1 & 0 & -1 \\ 0 & 1 & 1 & 1 & 1 \\ 0 & 1 & -1 & 1 & -1 \end{bmatrix}.\end{aligned} \tag{26}$$

In the model, n_0 is the only conserved moment and the temperature T is computed by

$$\sigma T \equiv n_0 = \sum_{i=0}^{4} g_i. \tag{27}$$

The equilibrium moments $\left\{n_i^{eq}\middle|\, i = 0, 1, \ldots, 4\right\}$ for the moments $\{n_i|\, i = 0, 1, \ldots, 4\}$ are defined as

$$n_0^{eq} = \sigma T, \qquad n_1^{eq} = u_x T, \qquad n_2^{eq} = u_y T, \qquad n_3^{eq} = \varpi\sigma T, \qquad n_4^{eq} = 0, \tag{28}$$

where $\varpi \in (0, 1)$ is a parameter of the model. The relaxation matrix $\mathbf{Q}$ is given by

$$\mathbf{Q} = \begin{bmatrix} \zeta_0 & 0 & 0 & 0 & 0 \\ 0 & \zeta_{xx} & \zeta_{xy} & 0 & 0 \\ 0 & \zeta_{xy} & \zeta_{yy} & 0 & 0 \\ 0 & 0 & 0 & \zeta_3 & 0 \\ 0 & 0 & 0 & 0 & \zeta_4 \end{bmatrix}. \tag{29}$$

For incompressible thermal problems with isotropic thermal diffusivity considered in this work, the relaxation matrix $\mathbf{\Omega}$ is diagonal one given by $\mathbf{\Omega} = \text{diag}\,(\zeta_0, \zeta_\alpha, \zeta_\alpha, \zeta_3, \zeta_4)$ ($\zeta_{xx} = \zeta_{yy} = \zeta_\alpha$ and $\zeta_{xy} = 0$).

The equilibrium distribution function g_i^{eq} ($\mathbf{g}^{eq} = \mathbf{N}^{-1}\mathbf{n}^{eq}$) in the velocity space is given by

$$g_i^{eq} = \begin{cases} (1-\varpi)\,\sigma T, & i = 0, \\ \dfrac{1}{4}\varpi\sigma T + \dfrac{1}{2}\,(\mathbf{e}_i \cdot \mathbf{u})\,T, & i = 1\text{–}4. \end{cases} \tag{30}$$

Through the Chapman–Enskog analysis of the MRT-LB equation (23), the following macroscopic equation can be obtained [48]

$$\partial_t\,(\sigma T) + \nabla \cdot (uT) = \nabla \cdot \left[\alpha_e \nabla T + \delta_t \left(\zeta_\alpha^{-1} - 0.5\right) \in \partial_{t_1}\,(\mathbf{u}T)\right], \tag{31}$$

where $\alpha_e = \sigma c_{sT}^2\,(\tau_T - 0.5)\,\delta_t$ is the effective thermal diffusivity ($\zeta_{1,2} = \zeta_\alpha = 1/\tau_T$), in which $c_{sT}^2 = c^2\varpi/2 = \varpi/2$ (c_{sT} is the sound speed of the D2Q5 model). In most cases, the second term in the bracket on the right-hand side of Eq. (31) can be neglected for incompressible flows, then Eq. (31) reduces to the temperature Eq. (3).

3.2.2. Finite difference scheme

In this subsection, the finite difference scheme [42] for the temperature field is briefly described. With a constant effective thermal diffusivity, Eq. (3) can be solved by the following finite difference equation:

$$T\,(\mathbf{x}, t + \delta_t) = T\,(\mathbf{x}, t) + \frac{1}{\sigma}\left[-\mathbf{u} \cdot \nabla T\,(\mathbf{x}, t) + \alpha_e \nabla^2 T\,(\mathbf{x}, t)\right]. \tag{32}$$

Note that if the effective thermal diffusivity α_e is variable, the term $\nabla \cdot (\alpha_e \nabla T)$ in Eq. (3) should be rewritten as $\nabla \cdot (\alpha_e \nabla T) = \nabla \alpha_e \cdot \nabla T + \alpha_e \nabla^2 T$. The finite difference operators corresponding to the D2Q9 model are given as follows ($\delta_x = \delta_t = 1$) [42]:

$$\partial_x T = T_{i+1,j} - T_{i-1,j} - \frac{1}{4}\left(T_{i+1,j+1} - T_{i-1,j+1} + T_{i+1,j-1} - T_{i-1,j-1}\right), \tag{33}$$

$$\partial_y T = T_{i,j+1} - T_{i,j-1} - \frac{1}{4}\left(T_{i+1,j+1} - T_{i+1,j-1} + T_{i-1,j+1} - T_{i-1,j-1}\right), \tag{34}$$

$$\nabla^2 T = 2\left(T_{i+1,j} + T_{i-1,j} + T_{i,j+1} + T_{i,j-1}\right) - \frac{1}{2}\left(T_{i+1,j+1} + T_{i-1,j+1} + T_{i-1,j-1} + T_{i+1,j-1}\right) - 6T_{i,j}. \tag{35}$$

Substituting Eqs. (33)–(35) into Eq. (32), the temperature at the time level $t + \delta_t$ can be obtained.

Finally, the D2Q9 MRT-LB equation (8) with the D2Q5 MRT-LB equation (23) constitute model I (DDF-MRT model), and the D2Q9 MRT-LB equation (8) with the finite difference scheme (32) constitute model II (hybrid MRT-FDM model), which can be used to simulate convection heat transfer problems in porous media at the REV scale.

4. Numerical simulations and discussions

In this section, numerical simulations of the mixed convection flow in a porous channel and natural convection flow in a porous cavity are carried out to demonstrate the effectiveness and accuracy of the present MRT-LB method. In simulations, we set $\rho_0 = 1$, $\delta_t = \delta_x = \delta_y = 1$ ($c = 1$), $\varpi = 1/2$ ($c_{sT}^2 = c/4 = 1/4$), $J = 1$, $\sigma = 1$, and $\alpha_e/\alpha = 1$. The free relaxation parameters are chosen as follows: $s_0 = s_1 = s_2 = 1$, $s_3 = 1.6$, $s_6 = s_7 = s_q = 1.2$, $s_8 = 1.8$, $\zeta_0 = 1$, and $\zeta_3 = \zeta_4 = 1.5$. Unless otherwise specified, the non-equilibrium extrapolation scheme [53] is employed to treat the velocity and temperature boundary conditions in simulations.

4.1. Mixed convection flow in a porous channel

In this subsection, numerical simulations of the mixed convection flow in a porous channel are carried out to test the numerical stability of the MRT-LB method. The height and length of the porous channel are H and L, respectively. The upper wall is hot ($T = T_h$) and moves along the x-direction with a uniform velocity u_0, while the bottom wall is cold ($T = T_c$) and a constant normal flow of fluid is injected (with a uniform velocity v_0) through the bottom wall. Without the nonlinear inertia term ($F_\phi = 0$), the flow is governed by the following equations (at the steady state) [36]:

$$\frac{u_y}{\phi}\frac{\partial u_x}{\partial y} = \upsilon_e \frac{\partial^2 u_x}{\partial y^2} - \frac{\phi \upsilon}{K} u_x, \tag{36}$$

$$\frac{1}{\rho_0}\frac{\partial p}{\partial y} = g\beta\,(T - T_0) - \frac{\upsilon}{K} u_y + a_y, \tag{37}$$

$$u_y \frac{\partial T}{\partial y} = \nabla \cdot (\alpha_e \nabla T)\,, \tag{38}$$

where $T_0 = (T_h + T_c)/2$ is the reference temperature, and a_y is the external force in the y-direction:

$$a_y = \frac{\upsilon}{K} v_0 - g\beta\Delta T \left[\frac{\exp(y v_0/\alpha_e) - 1}{\exp(H v_0/\alpha_e) - 1}\right]. \tag{39}$$

The analytical solutions of Eqs. (36)–(38) are given by [36]

$$u_x = u_0 \exp\left[\vartheta_1\left(\frac{y}{H} - 1\right)\right] \frac{\sinh(\vartheta_2 \cdot y/H)}{\sinh(\vartheta_2)}, \qquad u_y = v_0, \tag{40}$$

$$T = T_c + \Delta T \frac{\exp(PrRe \cdot y/H) - 1}{\exp(PrRe) - 1}, \tag{41}$$

where $Re = H v_0/\upsilon$ is the Reynolds number, $\Delta T = T_h - T_c$ is the temperature difference, the two parameters ϑ_1 and ϑ_2 in Eq. (40) are given by

$$\vartheta_1 = \frac{Re}{2\phi J}, \qquad \vartheta_2 = \frac{1}{2\phi J}\sqrt{Re^2 + \frac{4\phi^3 J}{Da}}. \tag{42}$$

In our simulations, we set $Ra = 100$, $Re = 5$, $Pr = 1$, $\phi = 0.6$, $Da = 0.01$, and a grid size of $N_x \times N_y = 32 \times 32$ is employed. The relaxation times τ_υ and τ_T can be determined by

$$\tau_\upsilon = \frac{1}{2} + \frac{JH v_0}{c_s^2 Re \delta_t}, \qquad \tau_T = \frac{1}{2} + \frac{\gamma c_s^2 (\tau_\upsilon - 0.5)}{J\sigma c_{sT}^2 Pr}, \tag{43}$$

respectively. Periodic boundary conditions are imposed at the inlet and outlet of the channel. The velocity and temperature profiles predicted by the MRT-LB method are in excellent agreement with the analytical ones, but the results are not shown here for the sake of brevity.

In what follows, we will confirm that the present MRT-LB model is more stable than the BGK-LB model [36] by comparing the results obtained by the present method with those obtained by the BGK-LB model [36] at low viscosities ($\upsilon = 5.0 \times 10^{-4}$ and 1.0×10^{-4}). The simulation results are shown in Figs. 1 and 2. It can be seen from Fig. 1(a) that the BGK-LB model is numerically unstable at $\upsilon = 5 \times 10^{-4}$ ($\tau_\upsilon = 0.5015$), while the present MRT-LB model is stable (see Fig. 1(b) and (c)) and can give accurate results at the steady state (see Fig. 1(d) and (e)), which demonstrates that the present MRT-LB model is indeed more stable that the BGK-LB model. To strength the above statement, we further reduce the viscosity to a smaller value, for example $\upsilon = 1.0 \times 10^{-4}$ ($\tau_\upsilon = 0.5003$), and find that the present MRT-LB model still works very well (see Fig. 2). Moreover, the better numerical stability of the present MRT-LB model at low thermal diffusivities is also demonstrated since the Prandtl number is 1.0 in simulations. By separating the relaxation rates of the conserved and non-conserved moments, the MRT collision model can significantly improve the numerical stability of the LB schemes.

4.2. Natural convection flow in a porous cavity

Natural convection flow in a fluid-saturated porous cavity has been studied extensively by many researchers [6,36,37,39]. The top and bottom walls of the cavity are adiabatic, while the left and right walls are kept at constant temperatures T_h and T_c ($T_h > T_c$), respectively. The average Nusselt number $\overline{Nu}$ of the left (or right) wall is defined by

$$\overline{Nu} = \frac{1}{H}\int_0^H Nu(y)\mathrm{d}y, \tag{44}$$

where $Nu(y) = -L(\partial T/\partial x)_{\text{wall}}/\Delta T$ is the local Nusselt number, $\Delta T = T_h - T_c$ is the temperature difference, H and L are the height and width of the cavity ($H/L = 1$), respectively. The reference temperature is $T_0 = (T_h + T_c)/2$. According to Refs. [39,48,51], the relaxation times τ_υ and τ_T can be determined by

$$\tau_\upsilon = \frac{1}{2} + \frac{MaJL\sqrt{3Pr}}{c\delta_t\sqrt{Ra}}, \qquad \tau_T = \frac{1}{2} + \frac{\gamma c_s^2 (\tau_\upsilon - 0.5)}{J\sigma c_{sT}^2 Pr}, \tag{45}$$

respectively, where $Ma = u_c/c_s$ is the Mach number, in which $u_c = \sqrt{g\beta\Delta TL}$ is the characteristic velocity. For incompressible porous flows considered in this work, Ma is set to be 0.1 in simulations.

Numerical simulations are carried out for a wide range of Rayleigh numbers, Darcy numbers and porosities. The grid sizes of 128×128, 192×192, and 256×256 are adopted for $Da = 10^{-2}$, 10^{-4}, and 10^{-6}, respectively. Fig. 3 illustrates the streamlines and isotherms obtained by model II at a fixed Darcy–Rayleigh number Ra^* ($Ra^* = RaDa$) with $Pr = 1.0$ and $\phi = 0.4$. From Fig. 3 we can observe that for low Da, the isotherms converge at the bottom corner of the hot wall and the top corner of the cold wall, and for the flow field, the streamlines crowd near the hot and cold walls. As Da decreases, the velocity and thermal boundary layers near the vertical walls become thinner. For high Da (non-Darcy flow), more convective mixing occurs in the interior of the cavity, and the isotherms are less crowded near the bottom corner of the hot wall and the

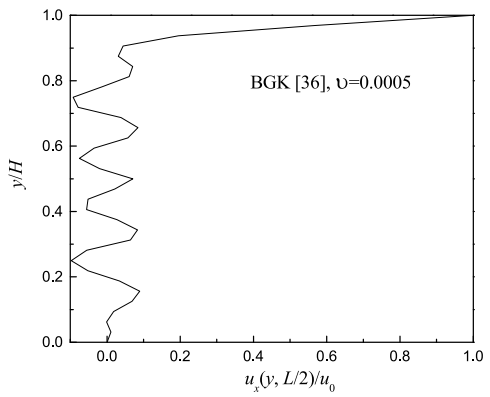

(a) BGK [36], $t = 2200\delta_t$, $\tau_\upsilon = 0.5015$.

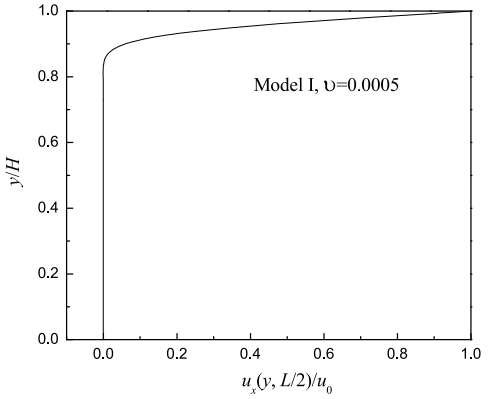

(b) Model I, $t = 2200\delta_t$, $\tau_\upsilon = 0.5015$.

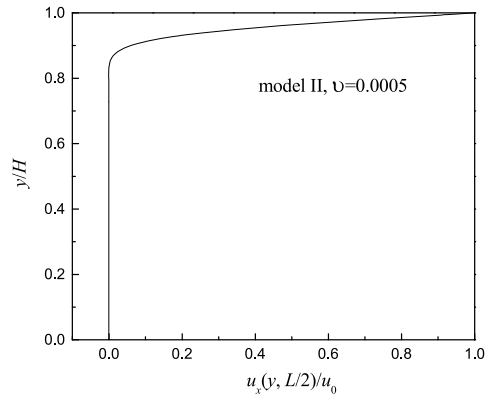

(c) Model II, $t = 2200\delta_t$, $\tau_\upsilon = 0.5015$.

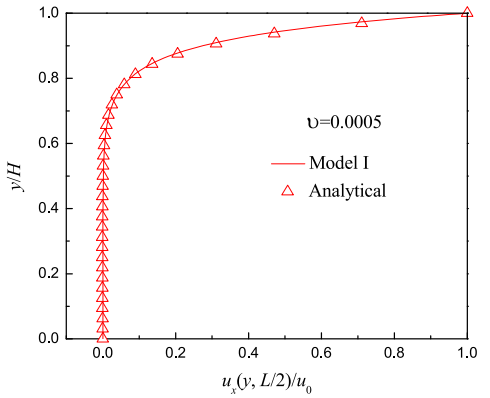

(d) Model I, steady-state, $\tau_\upsilon = 0.5015$.

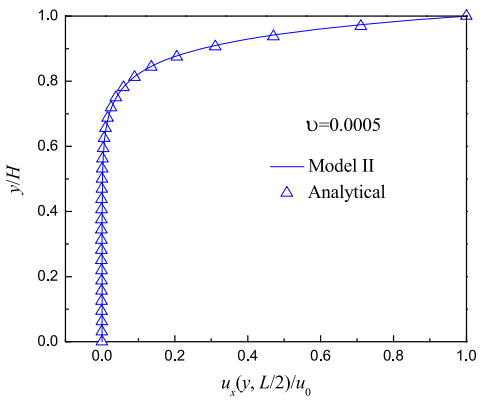

(e) Model II, steady-state, $\tau_\upsilon = 0.5015$.

Fig. 1. Velocity profiles of the mixed convection flow in a porous channel at $Re = 5$, $Ra = 100$, $Pr = 1$, $\phi = 0.6$, $Da = 0.01$ with a low viscosity $\upsilon = 5.0 \times 10^{-4}$ ($\tau_\upsilon = 0.5015$).

top corner of the cold wall. The above observations indicate that at a fixed Ra^*, the heat transport in the Darcy flow regime is much higher than that in the non-Darcy flow regime.

The vertical velocity and temperature profiles at the midheight of the cavity obtained by model I and model II are presented in Fig. 4. The results obtained by model I and model II are almost the same. From Fig. 4(a) it can be observed that the vertical velocity has a positive peak near the hot wall and a negative peak near the cold wall, and the values of the vertical velocity are rather small in the core region of the cavity. At a fixed value of Ra^*, the positive peak and negative peak of the vertical velocity profile climb up and become more and more sharp as Da decreases. In Fig. 4(b), the temperature

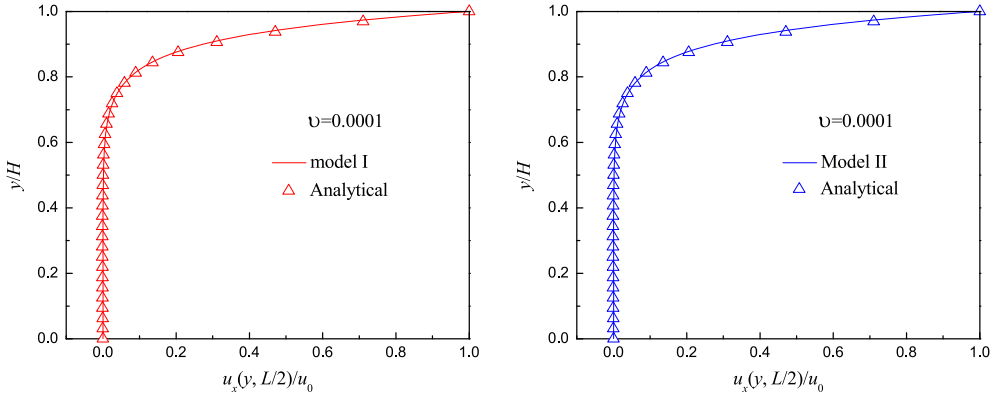

(a) Model I, steady-state, $\tau_\upsilon = 0.5003$. (b) Model II, steady-state, $\tau_\upsilon = 0.5003$.

Fig. 2. Velocity profiles of the mixed convection flow in a porous channel at $Re = 5$, $Ra = 100$, $Pr = 1$, $\phi = 0.6$, $Da = 0.01$ with a low viscosity $\upsilon = 1.0 \times 10^{-4}(\tau_\upsilon = 0.5003)$.

Table 1
Comparisons of the average Nusselt numbers for various values of Ra, ϕ and Da with $Pr = 1.0$.

Da	Ra	$\phi = 0.4$			$\phi = 0.6$			$\phi = 0.9$		
		Ref. [6]	Model I	Model II	Ref. [6]	Model I	Model II	Ref. [6]	Model I	Model II
10^{-2}	10^3	1.01	1.0075	1.0077	1.015	1.0117	1.0121	1.023	1.0170	1.0176
	10^4	1.408	1.3616	1.3608	1.530	1.4931	1.4921	1.64	1.6353	1.6328
	10^5	2.983	3.0059	2.9921	3.555	3.4397	3.4371	3.91	3.9371	3.9148
	5×10^5	4.99	5.0091	4.9822	5.740	5.7883	5.7570	6.70	6.6310	6.5770
10^{-4}	10^5	1.067	1.0661	1.0643	1.071	1.0670	1.0673	1.072	1.0699	1.0697
	10^6	2.55	2.6053	2.5952	2.725	2.7142	2.7044	2.740	2.7968	2.7901
	10^7	7.81	7.7765	7.7527	8.183	8.4956	8.5372	9.202	9.2456	9.2664
10^{-6}	10^7	1.079	1.0760	1.0695	1.079	1.0765	1.0698	1.08	1.0778	1.0701
	10^8	2.97	3.0205	3.0382	2.997	3.0365	3.0582	3.00	3.0431	3.0704
	10^9	11.46	11.6987	11.6642	11.79	11.9861	12.02	12.01	12.1590	12.2091

distributions along the horizontal midline are presented. It is seen that the temperature distribution at $Da = 10^{-6}$ is similar to that at $Da = 10^{-4}$ for a fixed value of Ra^*. As Da increases, the temperature gradient near the wall decreases due to the decreased convection effect caused by lower fluid velocity. The observed phenomena from the velocity and temperature profiles agree well with those reported in Refs. [6,36].

To quantify the results, the average Nusselt numbers of the hot wall are calculated and listed in Table 1. From the predicted results, the following trends can be observed: (i) for a given Ra^*, $\overline{Nu}$ increases with ϕ because the inertial and nonlinear drag forces are less significant for higher porosity; (ii) for low Ra^* ($\leq$10), $\overline{Nu}$ is almost independent of the individual values of Ra, Da, and ϕ; (iii) for a given Ra and ϕ, $\overline{Nu}$ increases with Da due to the higher permeability of the porous medium ($K = DaL^2$) which results in higher fluid velocity; (iv) for a fixed Ra^*, the heat transport in the Darcy flow regime is much higher than that in the non-Darcy flow regime. The numerical results obtained by Nithiarasu et al. [6] using the finite element method are also included in Table 1 for comparison. It can be seen that the numerical results predicted by the present method agree well with those reported in the literature. Furthermore, it is found that model II is computationally more efficient than model I. The computational time of model II is about 20% less than that of model I (e.g., for $Ra = 10^6$, $\phi = 0.6$, and $Da = 10^{-4}$, the CPU times of model I and model II are 21 556 s and 17 103 s at $t = 6.0 \times 10^5 \delta_t$, respectively).

5. Conclusions

A non-orthogonal MRT-LB method has been developed for simulating natural convection heat transfer in porous media at the REV scale based on the generalized non-Darcy model. In the method, two different LB models are constructed: one is constructed in the framework of the DDF approach, and the other is constructed in the framework of the hybrid approach. The key point of the present method is that the effect of the porous media is considered by introducing the porosity into the equilibrium moments and adding a forcing term, which accounts for the linear and nonlinear drag forces of the solid matrix, to the MRT-LB equation of the flow field in the moment space. In particular, the transformation matrices used in the MRT-LB models are non-orthogonal matrices. The present method can be used to study porous flows with a constant or variable porosity.

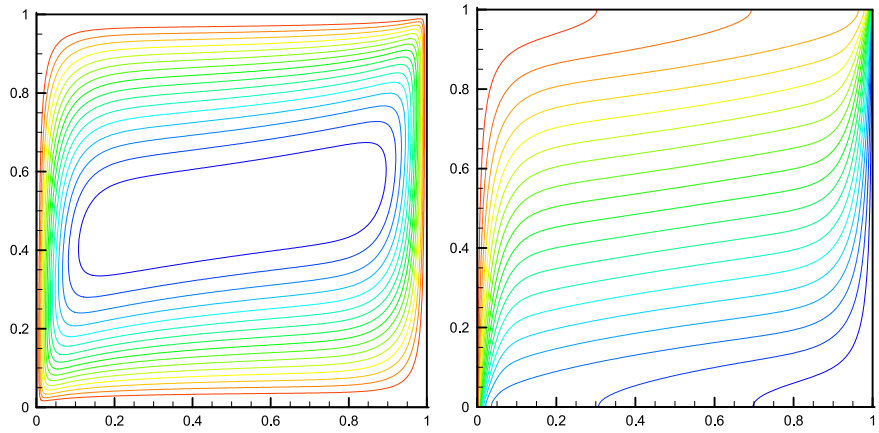

(a) $Da = 10^{-6}$, $Ra = 10^{9}$.

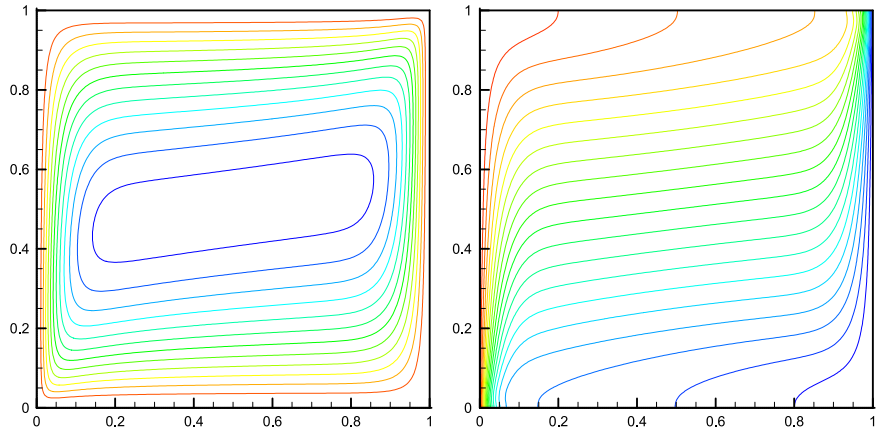

(b) $Da = 10^{-4}$, $Ra = 10^{7}$.

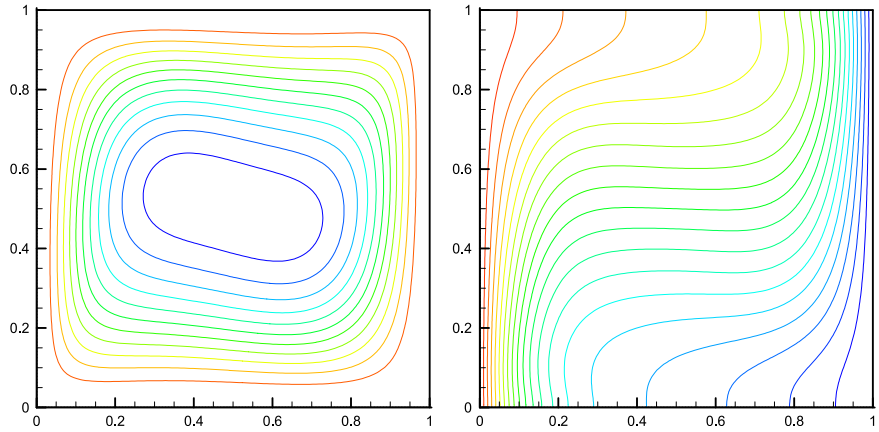

(c) $Da = 10^{-2}$, $Ra = 10^{5}$.

Fig. 3. Streamlines (left) and isotherms (right) of natural convection flow in a porous cavity for $Pr = 1.0$ and $\phi = 0.4$ (model II).

Numerical simulations of mixed convection flow in a porous channel and natural convection flow in a porous cavity are carried out to validate the present method. The numerical results are in good agreement with the analytical solutions and/or other results reported in previous studies, demonstrating that the present method can be served as a numerically accurate and computationally efficient numerical method for studying convection heat transfer in porous media. Furthermore, it is found that the non-orthogonal MRT-LB method is more stable than the BGK-LB method at low viscosities, which makes the present method more useful in practical applications.

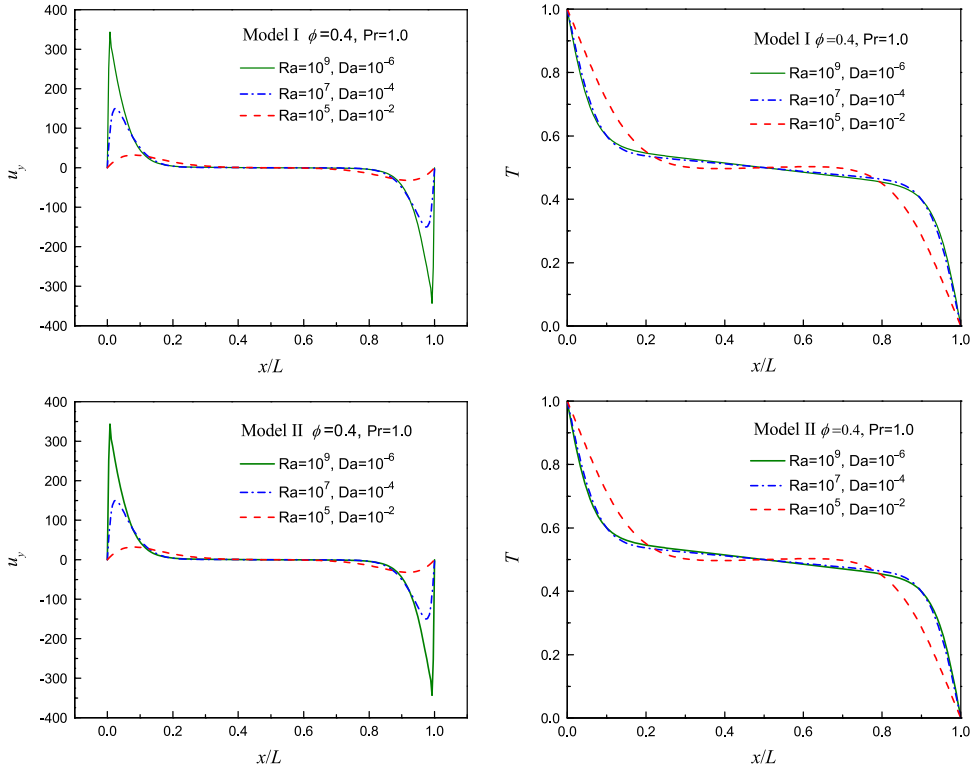

(a) Velocity profiles. (b) Temperature profiles.

Fig. 4. Vertical velocity (a) and temperature (b) profiles at the midheight of the porous cavity.

Acknowledgments

This work is supported by the Key Project of National Natural Science Foundation of China (No. 51436007) and the National Key Basic Research Program of China (973 Program) (2013CB228304).

References

[1] P. Cheng, Heat transfer in geothermal systems, Adv. Heat Transfer 14 (1978) 1–105.
[2] D.A. Nield, A. Bejan, Convection in Porous Media, fourth ed., Springer, New York, 2013.
[3] P. Cheng, Thermal dispersion effects in non-Darcian convective flows in a saturated porous medium, Lett. Heat Mass Transfer 8 (4) (1981) 267–270.
[4] K. Vafai, Convective flow and heat transfer in variable-porosity media, J. Fluid Mech. 147 (1984) 233–259.
[5] C.T. Hsu, P. Cheng, Thermal dispersion in a porous medium, Int. J. Heat Mass Transfer 33 (8) (1990) 1587–1597.
[6] P. Nithiarasu, K.N. Seetharamu, T. Sundararajan, Natural convective heat transfer in a fluid saturated variable porosity medium, Int. J. Heat Mass Transfer 40 (16) (1997) 3955–3967.
[7] G.R. McNamara, G. Zanetti, Use of the Boltzmann equation to simulate lattice-gas automata, Phys. Rev. Lett. 61 (20) (1988) 2332–2335.
[8] F.J. Higuera, J. Jimenez, Boltzmann approach to lattice gas simulation, Europhys. Lett. 9 (7) (1989) 663–668.
[9] F.J. Higuera, S. Succi, R. Benzi, Lattice gas dynamics with enhanced collisions, Europhys. Lett. 9 (7) (1989) 345–349.
[10] H. Chen, S. Chen, W.H. Matthaeus, Recovery of the Navier–Stokes equations using a lattice-gas Boltzmann method, Phys. Rev. A 45 (8) (1992) R5339–R5342.
[11] Y.H. Qian, D. d'Humières, P. Lallemand, Lattice BGK models for Navier–Stokes equation, Europhys. Lett. 17 (6) (1992) 479–484.
[12] U. Frisch, B. Hasslacher, Y. Pomeau, Lattice-gas automata for the Navier–Stokes equation, Phys. Rev. Lett. 56 (1986) 1505–1508.
[13] R. Benzi, S. Succi, M. Vergassola, The lattice Boltzmann equation: theory and applications, Phys. Rep. 222 (3) (1992) 145–197.
[14] S. Succi, The Lattice Boltzmann Equation for Fluid Dynamics and Beyond, Clarendon Press, Oxford, 2001.
[15] Y.L. He, Y. Wang, Q. Li, Lattice Boltzmann Method: Theory and Applications, Science Press, Beijing, 2009.
[16] A.A. Mohamad, Lattice Boltzmann Method: Fundamentals and Engineering Applications with Computer Codes, Springer Science & Business Media, 2011.
[17] S. Gong, P. Cheng, Lattice Boltzmann simulation of periodic bubble nucleation, growth and departure from a heated surface in pool boiling, Int. J. Heat Mass Transfer 64 (2013) 122–132.
[18] Y. Wang, S. Elghobashi, On locating the obstruction in the upper airway via numerical simulation, Respir. Physiol. Neurobiol. 193 (2014) 1–10.
[19] Q. Liu, Y.L. He, Double multiple-relaxation-time lattice Boltzmann model for solid–liquid phase change with natural convection in porous media, Physica A 438 (2015) 94–106.
[20] Q. Li, Q.J. Kang, M.M. Francois, Y.L. He, K.H. Luo, Lattice Boltzmann modeling of boiling heat transfer: The boiling curve and the effects of wettability, Int. J. Heat Mass Transfer 85 (2015) 787–796.
[21] Y. Wang, D.K. Sun, Y.L. He, W.Q. Tao, Lattice Boltzmann study on thermoacoustic onset in a Rijke tube, Eur. Phys. J. Plus 130 (1) (2015) 9.
[22] Q. Li, K.H. Luo, Q.J. Kang, Y.L. He, Q. Chen, Q. Liu, Lattice Boltzmann methods for multiphase flow and phase-change heat transfer, Prog. Energy Combust. Sci. 52 (2016) 62–105.
[23] S. Succi, Lattice Boltzmann across scales: from turbulence to DNA translocation, Eur. Phys. J. B 64 (3–4) (2008) 471–479.

[24] S. Succi, Lattice Boltzmann 2038, Europhys. Lett. 109 (5) (2015) 50001.
[25] S. Succi, E. Foti, F. Higuera, Three-dimensional flows in complex geometries with the lattice Boltzmann method, Europhys. Lett. 10 (5) (1989) 433.
[26] A. Cali, S. Succi, A. Cancelliere, R. Benzi, M. Gramignani, Diffusion and hydrodynamic dispersion with the lattice Boltzmann method, Phys. Rev. A 45 (8) (1992) 5771–5774.
[27] G.H. Tang, W.Q. Tao, Y.L. He, Gas slippage effect on microscale porous flow using the lattice Boltzmann method, Phys. Rev. E 72 (5) (2005) 056301.
[28] Q. Kang, P.C. Lichtner, D. Zhang, An improved lattice Boltzmann model for multicomponent reactive transport in porous media at the pore scale, Water Resour. Res. 43 (12) (2007).
[29] P. Prestininzi, A. Montessori, M. La Rocca, S. Succi, Reassessing the single relaxation time lattice Boltzmann method for the simulation of Darcy's flows, Internat. J. Modern Phys. C 27 (04) (2016) 1650037.
[30] M.A.A. Spaid, F.R. Phelan Jr., Lattice Boltzmann methods for modeling microscale flow in fibrous porous media, Phys. Fluids 9 (9) (1997) 2468–2474.
[31] O. Dardis, J. McCloskey, Lattice Boltzmann scheme with real numbered solid density for the simulation of flow in porous media, Phys. Rev. E 57 (1998) 4834–4837.
[32] D.M. Freed, Lattice-Boltzmann method for macroscopic porous media modeling, Internat. J. Modern Phys. C 9 (08) (1998) 1491–1503.
[33] Q. Kang, D. Zhang, S. Chen, Unified lattice Boltzmann method for flow in multiscale porous media, Phys. Rev. E 66 (2002) 056307.
[34] Z. Guo, T.S. Zhao, Lattice Boltzmann model for incompressible flows through porous media, Phys. Rev. E 66 (2002) 036304.
[35] A. Zarghami, C. Biscarini, S. Succi, S. Ubertini, Hydrodynamics in porous media: A finite volume lattice Boltzmann study, J. Sci. Comput. 59 (1) (2014) 80–103.
[36] Z. Guo, T.S. Zhao, A lattice Boltzmann model for convection heat transfer in porous media, Numer. Heat Transfer B 47 (2005) 157–177.
[37] T. Seta, E. Takegoshi, K. Okui, Lattice Boltzmann simulation of natural convection in porous media, Math. Comput. Simulation 72 (2) (2006) 195–200.
[38] D. Gao, Z. Chen, Lattice Boltzmann simulation of natural convection dominated melting in a rectangular cavity filled with porous media, Int. J. Therm. Sci. 50 (2011) 493–501.
[39] Q. Liu, Y.L. He, Q. Li, W.Q. Tao, A multiple-relaxation-time lattice Boltzmann model for convection heat transfer in porous media, Int. J. Heat Mass Transfer 73 (2014) 761–775.
[40] D. d'Humières, Generalized lattice-Boltzmann equations, in: B.D. Shizgal, D.P. Weaver (Eds.), Rarefied Gas Dynamics: Theory and Simulations, in: Prog. Astronaut. Aeronaut., vol. 159, AIAA, Washington, DC, 1992, pp. 450–458.
[41] P. Lallemand, L.-S. Luo, Theory of the lattice Boltzmann method: Dispersion, dissipation, isotropy, Galilean invariance, and stability, Phys. Rev. E 61 (2000) 6546–6562.
[42] P. Lallemand, L.-S. Luo, Theory of the lattice Boltzmann method: Acoustic and thermal properties in two and three dimensions, Phys. Rev. E 68 (3) (2003) 036706.
[43] Q. Li, Y.L. He, G.H. Tang, W.Q. Tao, Improved axisymmetric lattice Boltzmann scheme, Phys. Rev. E 81 (5) (2010) 056707.
[44] L.-S. Luo, W. Liao, X. Chen, Y. Peng, W. Zhang, Numerics of the lattice Boltzmann method: Effects of collision models on the lattice Boltzmann simulations, Phys. Rev. E 83 (5) (2011) 056710.
[45] I. Rasin, S. Succi, W. Miller, A multi-relaxation lattice kinetic method for passive scalar diffusion, J. Comput. Phys. 206 (2005) 453–462.
[46] H. Yoshida, M. Nagaoka, Multiple-relaxation-time lattice Boltzmann model for the convection and anisotropic diffusion equation, J. Comput. Phys. 229 (2010) 7774–7795.
[47] K.N. Premnath, S. Banerjee, Incorporating forcing terms in cascaded lattice Boltzmann approach by method of central moments, Phys. Rev. E 80 (3) (2009) 036702.
[48] Q. Liu, Y.L. He, D. Li, Q. Li, Non-orthogonal multiple-relaxation-time lattice Boltzmann method for incompressible thermal flows, Int. J. Heat Mass Transfer 102 (2016) 1334–1344.
[49] X. Shan, Simulation of Rayleigh-Bénard convection using a lattice Boltzmann method, Phys. Rev. E 55 (3) (1997) 2780–2788.
[50] X. He, S. Chen, G.D. Doolen, A novel thermal model for the lattice Boltzmann method in incompressible limit, J. Comput. Phys. 146 (1) (1998) 282–300.
[51] Q. Li, Y.L. He, Y. Wang, G.H. Tang, An improved thermal lattice Boltzmann model for flows without viscous heat dissipation and compression work, Internat. J. Modern Phys. C 19 (1) (2008) 125–150.
[52] S. Ergun, Fluid flow through packed columns, Chem. Eng. Prog. 48 (1952) 89–94.
[53] Z.L. Guo, C.G. Zheng, B.C. Shi, Non-equilibrium extrapolation method for velocity and pressure boundary conditions in the lattice Boltzmann method, Chin. Phys. 11 (4) (2002) 366–374.